Kramers doublet ground state in topological Kondo insulators

M. A. Griffith,[1] M. A. Continentino,[1] and T. O. Puel[2,3,1,*]

[1]*Centro Brasileiro de Pesquisas Físicas, Rua Xavier Sigaud 150, 22290-180 Rio de Janeiro, Brazil*

[2]*Beijing Computational Science Research Center, Haidian District, Beijing 100094, China*

[3]*CeFEMA, Instituto Superior Técnico, Universidade de Lisboa, Avenida Rovisco Pais, 1049-001 Lisboa, Portugal*

(Received 10 September 2018; published 6 February 2019)

We consider the simplest variant of a Kondo insulator where a doublet of localized f electrons hybridizes with spin-degenerate conduction electrons. We analyze the symmetries of f orbitals involved in the hybridization and point out that the effective four-band model of such systems provides further descriptions of clean Kondo insulators; namely the spin texture of the surface states is described by an integer winding number. We discuss general conditions for the appearance of topological nontrivial states and implications for rare-earth-based compounds. As an example, we derive the full phase diagram of tetragonal Kondo insulators. In particular, our findings describe the spin texture in the physically interesting nontrivial topological phase, i.e., when the bandwidth of conduction electrons sets the largest energy scale, and a new weak topological phase appears as a function of the normalized distance between the bands' center.

DOI: 10.1103/PhysRevB.99.075109

I. INTRODUCTION

Kondo insulators recently have attracted a lot of attention due to their promise to realize topological phases with a large bulk gap generated by strong electron correlations [1–8]. Different effective models have been proposed for several candidate materials, but not all of them are in a strong topological phase protected by a nontrivial $\mathbb{Z}_2$ invariant [9–11]. In the context of SmB_6, one promising candidate for a topological Kondo insulator, the consequences of mirror symmetries have been pointed out [12,13]. The latter allow for a refined topological characterization and are reflected in the surface-state spin structure; for instance, spin expectation values of surfaces were observable in SmB_6 from spin-resolved ARPES experiments [14]. Improving the topological characterization of Kondo insulators is, from a broader perspective, relevant for the identification of further promising materials.

In this work we revisit the simplest variant of a three-dimensional Kondo insulator where a doublet of localized f electrons hybridizes with spin-degenerate conduction electrons. We point out that not only the lattice symmetry of the material but also the symmetry of the f orbitals involved in the hybridization can allow for an improved characterization of the Kondo insulator, which results from a rotational invariance of the involved orbital wave functions. Specifically, we show that the surface-state spin texture in topological insulators involving localized Kramers doublets with the lowest angular momentum projection, $\Gamma^J_{1/2} = |J, m_J = \pm 1/2\rangle$, can be understood from a fine-tuned Hamiltonian characterized by an integer winding number. This work enlightens this connection and the conditions to relate this winding number to the spin texture of the $\mathbb{Z}_2$ Kondo insulators.

For tetragonal Kondo insulators we show that it is particularly useful when the bandwidth of conduction electrons sets the largest energy scale. On the other hand, when other than the $\Gamma^J_{1/2}$ doublet participates in the hybridization, it may only appear in a low hopping neighbor expansion; i.e., it is broken by higher-order neighbor contributions (which depend on both the involved doublet and crystal symmetry). This property, therefore, can only exist in those crystalline lattice structures that allow for a pure $\Gamma^J_{1/2}$ doublet in the ground state. We also identify the relevant point group symmetries for Kondo insulators involving doublets from the $J = 5/2$ and $7/2$ multiplets and discuss implications for rare-earth-based compounds.

II. MODEL

We start out from the simplest variant of a $3D$ Kondo insulator, where a spin-degenerate wide conduction band hybridizes with a narrow band formed by degenerate doublets $\Gamma^J = |J, \pm\rangle$ of nearly localized f electrons,

$$\hat{H} = \sum_{\boldsymbol{k}} \left(\sum_{\sigma=\uparrow,\downarrow} \varepsilon^c_{\boldsymbol{k}} c^\dagger_{\boldsymbol{k},\sigma} c_{\boldsymbol{k},\sigma} + \sum_{s=\pm} \varepsilon^f_{\boldsymbol{k}} f^\dagger_{\boldsymbol{k},s} f_{\boldsymbol{k},s} \right) + \sum_{\boldsymbol{k}} \sum_{\sigma=\uparrow,\downarrow} \sum_{s=\pm} (V_{\boldsymbol{k},\sigma s} c^\dagger_{\boldsymbol{k},\sigma} f_{\boldsymbol{k},s} + V^*_{\boldsymbol{k},\sigma s} f^\dagger_{\boldsymbol{k},s} c_{\boldsymbol{k},\sigma}). \quad (1)$$

Here $\varepsilon^{c,f}_{\boldsymbol{k}}$ are the energy dispersions of conduction and f electrons, respectively, and $V_{\boldsymbol{k},\sigma s}$ account for their hybridization. (Both $\varepsilon^f_{\boldsymbol{k}}$ and $V_{\boldsymbol{k},\sigma s}$ are considered as effective parameters that include effects from electron correlations. Treating correlations beyond the mean-field limit is very challenging, particularly in three dimensions. Most of these approaches consider one- or two-dimensional systems [15–21].) Throughout this work we always assume a sufficiently large crystal field, which separates a Kramers degenerate ground state from

*tharnier@csrc.ac.cn

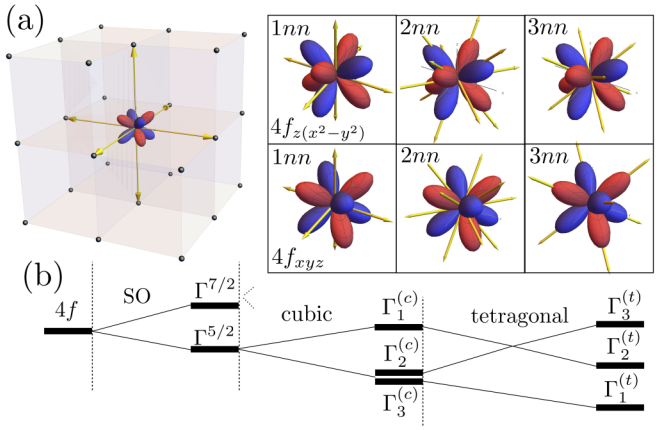

FIG. 1. The low-order neighbor expansion is illustrated in panel (a), where the arrows point to the next-neighbor directions in the cubic lattice, which is filled with the orbital configurations $4f_{xyz}$ and $4f_{z(x^2-y^2)}$. For the first next neighbors ($1nn$) one notices that their directions do not coincide with the atomic orbitals, while for $2nn$ and $3nn$ they coincide with $4f_{z(x^2-y^2)}$ and $4f_{xyz}$, respectively. Panel (b) shows the f-orbital degeneracy splitting caused by strong spin-orbit (SO) coupling followed by the crystalline field.

the 5/2 or 7/2 multiplet. While generally Γ^J is some linear combination of the angular momentum eigenstates $\Gamma^J_{m_J} \equiv |J, \pm m_J\rangle$, of specific interest to us are cases in which $\Gamma^J = \Gamma^J_{1/2}$. Figure 1(b) illustrates the crystal field splitting after the addition of spin-orbit coupling for the cubic and tetragonal structures, where $\Gamma^{(c),(t)}_{1,2,3}$ follow the notation in Ref. [3]; indeed the interesting ground state here is $\Gamma^{(t)}_1 = \Gamma^{5/2}_{1/2}$. Before we go into details, it is convenient to express Eq. (1) in the matrix form $\hat{H} = \sum_{\boldsymbol{k}} \Psi^\dagger_{\boldsymbol{k}} \mathcal{H}(\boldsymbol{k}) \Psi_{\boldsymbol{k}}$, where $\Psi^\dagger_{\boldsymbol{k}} = (c^\dagger_{\boldsymbol{k}\uparrow}, c^\dagger_{\boldsymbol{k}\downarrow}, f^\dagger_{\boldsymbol{k},+}, f^\dagger_{\boldsymbol{k},-})$ and

$$\mathcal{H}(\boldsymbol{k}) = \sum_{i=0}^{5} h_i(\boldsymbol{k}) \gamma_i, \tag{2}$$

with $h_{0,4}(\boldsymbol{k}) = (\varepsilon^c_{\boldsymbol{k}} \pm \varepsilon^f_{\boldsymbol{k}})/2$ and the remaining coefficient functions $h_i(\boldsymbol{k})$ defined by the hybridization elements $V_{\boldsymbol{k},\sigma s}$. Here $\gamma_0 = \mathbb{1}_4$ is the identity matrix and $\gamma_i = \sigma_i \otimes \tau_1$ (for $i = 1, 2, 3$), $\gamma_4 = \mathbb{1}_2 \otimes \tau_3$, and $\gamma_5 = \mathbb{1}_2 \otimes \tau_2$ are Dirac matrices satisfying the Clifford algebra $\{\gamma_a, \gamma_b\} = 2\delta_{ab}$, with Pauli matrices σ_i and τ_i operating in spin and orbital space, respectively. The general form of Eq. (2) is fixed by invariance under inversion, $\mathcal{I} = \sigma_0 \otimes \tau_3$, and time reversal, $\mathcal{T} = i\sigma_2 \otimes \tau_0 K$ (with K the complex conjugation) [22]. In some cases, the symmetry of participating f orbitals imposes an additional constraint to Eq. (2) as we are going to discuss next.

III. KRAMERS DOUBLETS $\Gamma^J_{1/2}$

To illustrate the point consider the hybridization block $c^\dagger_{\boldsymbol{k}} V_{m_J}(\boldsymbol{k}) f_{\boldsymbol{k}}$ for one of the Kramers doublets $\Gamma^{5/2}_{m_J}$. Following previous work [23] the 2×2 hybridization matrix reads

$$V_{n-\frac{1}{2}}(\boldsymbol{k}) = \begin{pmatrix} c_n \mathcal{Y}^{n-1}_3(\boldsymbol{k}) & \bar{c}_n \mathcal{Y}^{-n}_3(\boldsymbol{k}) \\ -\bar{c}_n \mathcal{Y}^{n}_3(\boldsymbol{k}) & -c_n \mathcal{Y}^{-n+1}_3(\boldsymbol{k}) \end{pmatrix}, \tag{3}$$

where c_n and $\bar{c}_n$ are purely real/imaginary numbers for n even/odd (as fixed by time-reversal symmetry) and

$$\mathcal{Y}^m_3(\boldsymbol{k}) = \sum_{\boldsymbol{R}\neq 0} v(|\boldsymbol{R}|)\, Y^m_3(\hat{\boldsymbol{R}}) e^{i\boldsymbol{k}\cdot\boldsymbol{R}}. \tag{4}$$

The sum in (4) runs over all neighbor sites $\boldsymbol{R}$; $Y^m_3(\hat{\boldsymbol{R}})$ are the spherical harmonic functions of f orbitals (with $\hat{\boldsymbol{R}}$ a unit vector), and coefficients $v(|\boldsymbol{R}|)$ depend on the neighbor distance. A similar expression (3) holds for the Kramers doublets $\Gamma^{7/2}_{m_J}$ [24] and the following discussion therefore applies to both multiplets $J = 5/2$ and $J = 7/2$.

Recalling that $\mathcal{Y}^{-m}_3(\hat{\boldsymbol{k}}) = (-1)^{m+1}[\mathcal{Y}^m_3(\hat{\boldsymbol{k}})]^*$, it is verified that Eq. (3) involves four independent real-valued functions. This is tantamount to noting that in general the hybridization block (3) requires in the Hamiltonian (2) a linear combination of the four matrices $\gamma_{1,2,3,5}$. A different situation, however, occurs for the Kramers doublet $\Gamma^J_{1/2}$ where the hybridization block involves the spherical harmonic $Y^0_3(\hat{\boldsymbol{R}})$ on its diagonal. Rotational symmetry of the latter implies that $c_n \mathcal{Y}^0_3(\boldsymbol{k})$ is a purely real-valued function and Eqs. (3) and (2) are spanned by only three out of the four independent γ matrices, i.e., $\gamma_{1,2,3}$ [25]. As we discuss in Sec. IV, the remaining matrix γ_5 is crucial to the improved characterization of the effective Hamiltonian (2).

Low neighbor expansion

We further notice that Eqs. (2) and (3) with only three of the four γ matrices may also appear in a low-order neighbor expansion for other than $m_J = 1/2$, but in this case it is not a robust constraint. For illustration consider Eqs. (3) and (4) in a cubic environment for the Kramers doublets $\Gamma^{5/2}_{3/2}$,

$$V_{\frac{3}{2}}(\boldsymbol{k}) \propto \begin{pmatrix} h_3(\boldsymbol{k}) - ih_5(\boldsymbol{k}) & h_1(\boldsymbol{k}) - ih_2(\boldsymbol{k}) \\ h_1(\boldsymbol{k}) + ih_2(\boldsymbol{k}) & -h_3(\boldsymbol{k}) - ih_5(\boldsymbol{k}) \end{pmatrix}. \tag{5}$$

While coefficient functions h_3, h_5 are nonvanishing already for nearest neighbors, h_1, h_2 become finite only starting from second- and third-order neighbors, respectively. This vanishing of h_1, h_2 is here traced back to the specific values of spherical harmonics $Y^{\pm 2}_3$ at the angles of the near-neighbor directions in the cubic lattice, as illustrated in Fig. 1(a) (i.e., zero for nearest and purely real for next-nearest neighbors), and also holds for tetragonal or orthorhombic but, e.g., not hexagonal lattices. The absence of h_5 in the case of the $\Gamma^J_{1/2}$ doublet discussed above, on the other hand, follows from the rotational symmetry of involved orbital functions and, therefore, applies for all neighbor contributions.

IV. FINE-TUNED HAMILTONIAN

We first note that in the translationally invariant insulating phase, i.e., clean system, one can always remove $h_0(\boldsymbol{k})$ from Eq. (2) without closing the gap. In addition, the topological phase diagram remains unaltered since eigenfunctions are not affected by terms proportional to identity. In general this procedure describes an adiabatic transformation; however, with the lack of γ_5 in the Hamiltonian, by removing $h_0(\boldsymbol{k})$ we are also adding an extra symmetry to the system, the chiral symmetry. Thus Kondo insulators involving hybridization with

a $\Gamma^J_{1/2}$ doublet are connected (besides nonadiabatically) to the fine-tuned Hamiltonian which possesses chiral symmetry, e.g.,

$$\gamma_5 \mathcal{H}_{\boldsymbol{k}} \gamma_5 = -\mathcal{H}_{\boldsymbol{k}}. \tag{6}$$

The consequences of this connection between $\mathbb{Z}_2$ Kondo insulators and the $\mathbb{Z}$ Hamiltonian (6), in class DIII [26], are analyzed through the example of tetragonal Kondo insulators discussed in the following.

Hamiltonians in class DIII are characterized by the winding number $N = \int \frac{d^3k}{48\pi^2} \epsilon^{ijk} \mathrm{tr}[\gamma_5 \mathcal{H}^{-1}(\partial_i \mathcal{H})\mathcal{H}^{-1}(\partial_j \mathcal{H})\mathcal{H}^{-1}(\partial_k \mathcal{H})]$ [27]; here summation over repeated indices is implicit, the integral extends over the first Brillouin zone, ϵ^{ijk} is the total antisymmetric Levi-Civita tensor, and $\partial_i \equiv \partial_{k_i}$. The winding number is related to the Brouwer index of the map $\boldsymbol{k} \mapsto (\boldsymbol{h}/|\boldsymbol{h}|)(\boldsymbol{k})$ with $\boldsymbol{h}^T = (h_1, h_2, h_3, h_4)$, i.e. [28],

$$N = \sum_{\boldsymbol{k} \in \boldsymbol{h}^{-1}(\boldsymbol{n}_0)} \mathrm{sgn}\det[\partial \boldsymbol{h}(\boldsymbol{k})], \tag{7}$$

where $\partial \boldsymbol{h}$ is the matrix with elements $(\partial \boldsymbol{h})_{ij} = \partial_i h_j$, and the sum is over points $\boldsymbol{k}$ in the Brillouin zone which map onto some (arbitrary) point $\boldsymbol{n}_0$ on the 3-sphere, $(\boldsymbol{h}/|\boldsymbol{h}|)(\boldsymbol{k}) = \boldsymbol{n}_0$. Notice that the winding counted by (7) cannot be changed as long as the chiral symmetry is preserved. That is, the topological properties are robust against time-reversal symmetry breaking perturbations that do not violate (6) [29].

A robust $\Gamma^J_{1/2}$-doublet ground state can only be realize in tetragonal and hexagonal lattices (as we will see), and the former are the most relevant for application of our results to known Kondo insulators. Concentrating then on tetragonal Kondo insulators with a $\Gamma^{5/2}_{1/2}$ doublet in the ground state, one finds (upon using parameters from the nearest-neighbor model [28])

$$N = \begin{cases} 2\,\mathrm{sgn}(v_\perp \delta), & |\Delta| < |\delta|, \\ -\mathrm{sgn}(v_\perp \delta), & 2 - |\delta| < |\Delta| < 2 + |\delta|, \\ 0, & \text{otherwise}, \end{cases} \tag{8}$$

where $\Delta = (\varepsilon_c - \varepsilon_f)/2(t^c_\parallel - t^f_\parallel)$ is the normalized distance between the center of the bands (i.e., $\varepsilon_c - \varepsilon_f$) and $v_\perp$ the hybridization intensity perpendicular to the symmetry plane. We also assumed that the anisotropy δ affects equally the hopping parameters $t^{c,f}_{\parallel/\perp}$ of c and f electrons within/perpendicular to the symmetry plane, i.e., $\delta = t^c_\perp / t^c_\parallel$ and $t^f_\perp = \delta t^f_\parallel$. The resulting phase diagram is shown in Fig. 2 for completely localized f electrons, $t^f_\parallel = t^f_\perp = 0$. Just below each winding number signalized in the phase diagram we also show the topological indices $\nu_0; (\nu_1\nu_2\nu_3)$ following Fu and Kane notation in Ref. [30]. The white regions are trivial phases with 0 in all topological invariants.

Spin texture

The topological nontrivial regions in Fig. 2 have the surface states ruled by the Fu and Kane indices; i.e., the indices $\nu_0 = 1$ and $\nu_0 = 0$ set the strong (gray) and weak (blue) topological phases of Kondo insulators respectively, with surface states in all directions, as discussed in [3,5,9]. The tetragonal structure

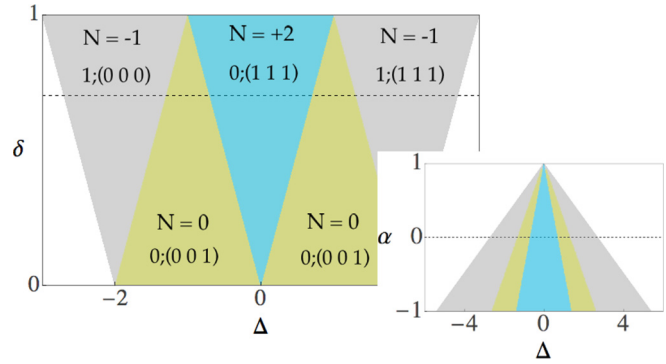

FIG. 2. Phase diagram of $3D$ Kondo insulators with tetragonal symmetry, derived from model Eq. (2) for the $\Gamma^{5/2}_{1/2}$ doublet in the nearest-neighbor approximation. Here $\delta = t^c_\perp/t^c_\parallel$, $\Delta = (\varepsilon_c - \varepsilon_f)/2(t^c_\parallel - t^f_\parallel)$, and we assumed $v_\perp > 0$, $t^f_\parallel = t^f_\perp = 0$. Gray regions correspond to strong topological phases with index $\nu_0 = 1$. Blue and green regions correspond to weak topological phases with indices $\nu_0; (\nu_1\nu_2\nu_3)$ equal to 0; (111) and 0; (001), respectively. White areas are trivial phases with zero to all topological invariants. The winding numbers $|N| = 2/0/1$ in blue/green/gray regions, respectively, characterize the spin texture of edge states in this system, as discussed in the main text. The dashed line indicates the value of δ used in the inset. Inset: Phase diagram for different (renormalized) bandwidths for f electrons $\alpha = t^f_\parallel / t^c_\parallel$ and fixed $\delta = 0.7$. The dashed line indicates the value used in the main figure.

pushes farther away the strong phase from the most relevant parameter regime and gives rise to an additional weak topological phase 0; (001) (green), with appearing surface states only on those surfaces aligned with z direction. Notice that increasing the hopping anisotropy ($\delta \to 0$), e.g., by application of uniaxial pressure, induces a phase transition into this new weak topological phase. Transitions between topological phases can also occur through correlation-induced renormalization of the f-electron dispersion [31]. The inset shows the phase diagram as a function of f-electron renormalized bandwidth $t^f_\parallel = \alpha t^c_\parallel$ at fixed $\delta = 0.7$ (delimitated by the dashed line in the main figure).

An interesting behavior is found in the most relevant parameter regime where the bandwidth of conduction electrons $t^c_\parallel$ sets the largest energy scale such that $|\Delta| \ll 1$. In this phase the winding number provides further description of the surface states; namely one finds $N \neq 0$ and 0; (111) (i.e., edge states in all surfaces and $|N| = 2$). Projecting the effective tetragonal Kondo Hamiltonians onto the surface states one finds that the winding number N in Eq. (7) allows us to infer the spin texture of the surface states [28]: specifically it counts the chiralities of the Dirac cones' pseudospin (spin texture); i.e., a weak topological phase with a vanishing winding number indicates an even number of Dirac cones with opposite chiralities, while a finite winding number indicates an even number of Dirac cones with the same chiralities. A similar property holds true for the strong topological phases with an odd number of Dirac cones, where the winding number counts the number of Dirac cones left unpaired (pairs of opposite chiralities), for example the phase with $|N| = 1$ in the phase diagram of Fig. 2. In the context of the low neighbor

TABLE I. Point group symmetries which separate a pure $\Gamma^J_{1/2}$ Kramers doublet with lowest projection of angular momentum from the spin-orbit multiplets $J = 5/2$ and $7/2$. This Kramers doublet can split from the $5/2$ sextet in all of the seven point group symmetries of the tetragonal lattice, or four out of the seven point group symmetries of the hexagonal lattice. In the case of the $7/2$ octet the Kramers doublet with the lowest projection of angular momentum can only split in four out of seven point group symmetries of the hexagonal lattice.

Crystal field	Point group	Multiplet
Tetragonal	$C_4, S_4, C_{4h}, D_4, C_{4v}, D_{2d}, D_{4h}$	5/2
Hexagonal	$C_6, C_{3h}, C_{6h}, D_{3h}$	5/2, 7/2

approximation, in Appendix E we given an example with the 4-band model of a cubic structure as described in Ref. [12].

Previous discussions of the edge states in the general chiral Hamiltonian Eq. (6) are found in Refs. [35–38]. In particular, it has been shown the interfaces that break time-reversal symmetry have their gapless edge states replaced by (gapped) nonsingular walls and solitons with spin texture protected by the chiral symmetry [36]. Finally, the appearance of spin texture in cubic structures based on the mirror symmetry is discussed in Refs. [12,13,28].

V. APPLICATIONS

Candidate compounds for topological Kondo insulators are formed from magnetic ions with ground states involving odd-parity orbitals. Concentrating onto the rare-earth 3^+ ions with partially filled $4f$ shell, Ce-, Sm-, and Yb-based materials are of potential interest. The ground-state Kramers doublet in the case of the former two compounds arises from the $5/2$ sextet and in the case of the latter from the $7/2$ octet. The necessary requirement for the appearance of a Kondo insulator as discussed here is then a crystal field which stabilizes the $\Gamma^J_{1/2}$ doublet in the ground state. Looking at representations of all possible point groups and their basis functions [39], we notice that from the f-electron multiplets a pure $\Gamma^J_{1/2}$ doublet only separates in tetragonal or hexagonal crystal symmetries. Specifically, the $\Gamma^{5/2}_{1/2}$ doublet is allowed as one possible ground state in all tetragonal lattices and some of the hexagonal lattices, while the $\Gamma^{7/2}_{1/2}$ doublet can only be a ground state in some of the hexagonal lattices. Table I summarizes the possible point group symmetries of lattices allowing for a Kondo insulator derived from the $5/2$ and $7/2$ multiplets, respectively. And we conclude that Ce- and Sm-based Kondo insulators can only have $\Gamma^J_{1/2}$-doublet ground state in tetragonal or hexagonal structures. One specific Ce compound with tetragonal point group symmetry D_{2d} to which our above analysis applies is $CeRu_4Sn_6$ [40]. Recent x-ray spectroscopy experiments in combination with band structure calculations indicate that the $\Gamma^{5/2}_{1/2}$ doublet is the lowest energy state and inversion of bands occurs [41–43]. Moreover, the $4f$ occupancy near to integer value $n_f \sim 1$ and the low dispersive f band put this material into the topologically interesting region $0;(111)$ with $|N| = 2$ of the phase diagram, Fig. 2. All known Sm-based Kondo insulators, on the other hand, have cubic symmetry and our analysis does not apply. Finally, Kondo insulators based on Yb can only exhibit the $\Gamma^J_{1/2}$-doublet ground state in the four hexagonal symmetries indicated in Table I. Among the established Yb-based Kondo insulators there are none with hexagonal symmetry; i.e., in these compounds further description of the spin texture can at most be realized in the low-order neighbor approximation. Recently, an interesting Yb compound with hexagonal symmetry, $YbNi_3X_9$ (X = Al, Ga), has been synthesized, but it appears to be metallic [44]. Besides the rare-earth elements, Kondo insulators may also be found in metal transition elements; for instance the new iridium-based compound Sr_2IrO_4 [45] has a narrow $5d$ band from Ir which hybridizes with the $4p$ band from oxygen. It also shows a $\Gamma^J_{1/2}$-doublet ground state and has a tetragonal lattice structure.

VI. CONCLUSIONS

We have studied $3D$ Kondo insulators where a wide conduction band hybridizes with a degenerate Kramers doublet of localized f electrons. We have shown that in cases where the doublet is that of the lowest angular momentum projection, $m_J = \pm 1/2$, the symmetry of orbitals involved allows for an improved description of the surface-state spin texture. Here the clean system is connected with a fine-tuned Hamiltonian in class DIII, which in turn is characterized by an integer winding number. In this case, the winding number distinguishes the chirality of Dirac cones at the surfaces, providing further information about the edge states.

As an example, in cases where the bandwidth of conduction electrons sets the largest energy scale, the tetragonal topological Kondo insulator is in a nontrivial phase $0;(111)$ with winding number $|N| = 2$, which means that we have two Dirac cones with the same chirality at each surface. Moreover, the phase diagram of this Kondo insulator shows a new weak topological phase when increasing the hopping anisotropy from the cubic to tetragonal structure. When other than the $m_J = \pm 1/2$ doublet is involved in the hybridization or when the crystalline field is other than one of those listed in Table I, such system may only appear in a low-order neighbor approximation.

Relevant crystal structures for this work are those which allow for a pure $\Gamma^J_{1/2}$ doublet in the ground state. In topological Kondo insulators involving Kramers doublets from the $7/2$ spin-orbit octet this ground state can only exist in some of the crystalline hexagonal lattices (see Table I). Kondo insulators forming from hybridization with a Kramers doublets from the $5/2$ sextet, on the other hand, can have it in all tetragonal and some of the hexagonal lattices. In practice, the crystal field splitting may not be strong enough to separate the ground state and (anisotropic) pressure may help to stabilize a topological phase. Finally, we have discussed several implications for the rare-earth compounds.

ACKNOWLEDGMENTS

The authors acknowledge extensive discussions with T. Micklitz, and T.O.P. thanks S. Kirchner for helpful comments. This work was supported by the Brazilian research agencies

TABLE II. Coefficient functions $h^n_{1,2,3,5}(\boldsymbol{k})$ parametrizing the hybridization matrix $V_{n-\frac{1}{2}}(\boldsymbol{k})$ for the $m_J = 1/2, 3/2$, and $5/2$ doublets of the $J = 5/2$ sextet in the nearest-neighbor approximation of a tetragonal lattice. Here $v_\parallel \equiv v(r^1_{x,y})$ and $v_\perp \equiv v(r^1_z)$ are the hybridization intensities within and perpendicular to the symmetry (x, y) plane, respectively.

$V_{n-\frac{1}{2}}$	h^n_1	h^n_2	h^n_3	h^n_5
$n = 1$	$v_\parallel \sin(k_x)$	$v_\parallel \sin(k_y)$	$-2v_\perp \sin(k_z)$	0
$n = 2$	0	0	$v_\parallel \sin(k_y)$	$v_\parallel \sin(k_x)$
$n = 3$	$-v_\parallel \sin(k_x)$	$v_\parallel \sin(k_y)$	0	0

CNPq and FAPERJ and the Chinese agency NSFC under Grants No. 11750110429 and No. U1530401.

APPENDIX A: WINDING NUMBER AND BROUWER INDEX

For convenience of the reader we here review the calculation of the winding number, $N = \int \frac{d^3k}{48\pi^2}\epsilon^{ijk}\,\mathrm{tr}[\gamma_5\mathcal{H}^{-1}(\partial_i\mathcal{H})\mathcal{H}^{-1}(\partial_j\mathcal{H})\mathcal{H}^{-1}(\partial_k\mathcal{H})]$, via the Brouwer degree, Eq. (7) in the main text. Starting out from the Hamiltonian matrix $\mathcal{H}(\boldsymbol{k}) = \sum_{i=1}^4 h_i(\boldsymbol{k})\gamma_i$ and the chiral symmetry operator $\gamma_5 = \gamma_1\gamma_2\gamma_3\gamma_4$, we use the anticommutation relation, $\{\gamma_a, \gamma_b\} = 2\delta_{ab}$, to simplify terms, e.g., $h_a h_b \gamma_a\gamma_b = \frac{1}{2}h_a h_b(\gamma_a\gamma_b + \gamma_b\gamma_a) = h_a h_b\delta_{ab} \equiv |h|^2$, etc. One then arrives at $N = \int \frac{d^3k}{48\pi^2} f^{ijk}_{abcd}\frac{h_a}{|h|^4}(\partial_i h_b)(\partial_j h_c)(\partial_k h_d)$, with $f^{ijk}_{abcd} = \epsilon^{ijk}\mathrm{tr}(\gamma_5\gamma_a\gamma_b\gamma_c\gamma_d)$, which can be cast into the form

$$N = \frac{1}{12\pi^2}\int \frac{1}{|h|^4}\epsilon^{abcd}h_a dh_b \wedge dh_c \wedge dh_d. \tag{A1}$$

Equation (A1) is the pull-back of the (normalized) volume form on the three-sphere, i.e., $N = \int h^*\omega_{S^3}$, where $\omega_{S^3} = \frac{1}{\mathrm{vol}(S^3)}\frac{1}{|k|^4}i_{k^a e_a}(dk_1 \wedge dk_2 \wedge dk_3 \wedge dk_4)$. The latter can be calculated from the Brouwer degree of the map $\boldsymbol{h}/|\boldsymbol{h}| : T^3 \to S^3$, $\boldsymbol{k} \mapsto (\boldsymbol{h}/|\boldsymbol{h}|)(\boldsymbol{k})$ with T^3 the $3D$ Brillouin zone torus and $\boldsymbol{h}^T = (h_1, h_2, h_3, h_4)$. The Brouwer degree counts the number of intersections of a ray through the origin and the oriented surface spanned by the map, as discussed in the main text.

APPENDIX B: HYBRIDIZATION MATRIX FOR THE 5/2 DOUBLETS IN TETRAGONAL CRYSTAL FIELD

Let us recall that matrices Eqs. (3) and (5) in the main text describe the hybridization

$$\hat{H}_V(\boldsymbol{k}) = \begin{pmatrix} c^\dagger_{\boldsymbol{k}\uparrow} & c^\dagger_{\boldsymbol{k}\downarrow}\end{pmatrix} V_{m_J}(\boldsymbol{k})\begin{pmatrix} f_{\boldsymbol{k},+m_J} \\ f_{\boldsymbol{k},-m_J}\end{pmatrix}, \tag{B1}$$

where $m_J = n - \frac{1}{2}$ from Eq. (3) in the main text. Concentrating then on Kramers doublets separating from the $J = 5/2$ sextet and a tetragonal symmetry, we find in the nearest-neighbor approximation the coefficient functions $h^n_{1,2,3,5}(\boldsymbol{k})$ summarized in Table II [see Eq. (4) in the main text]. This situation was also considered in Ref. [47] up to the first-next-neighbor approximation.

We notice that in the nearest-neighbor approximation hybridization with $m_J = 3/2$ and $5/2$ doublets does not open a gap in the spectrum and the system remains metallic. As discussed in the main text, vanishing coefficient functions for $m_J = 5/2$ and $7/2$ doublets are related to the specific values of spherical harmonics $Y_3^{\pm 2}$ at the angles of the nearest-neighbor directions, here in the tetragonal lattice. In the case of the $m_J = 1/2$ doublet, on the other hand, vanishing of h_5 is a consequence of the rotational symmetry of Y_3^0, and independent of the nearest-neighbor approximation.

TABLE III. Coefficient functions $h^n_{1,2,3,5}(\boldsymbol{k})$ as in Table II, now including next-nearest-neighbor contributions.

$V_{n-\frac{1}{2}}$	h^n_1	h^n_2	h^n_3	h^n_5
$n = 1$	$F_a \sin(k_x)$	$F_b \sin(k_y)$	$-F_c \sin(k_z)$	0
$n = 2$	0	$5F'_c \sin(k_z)$	$F_b \sin(k_y)$	$F_a \sin(k_x)$
$n = 3$	$-F'_a \sin(k_x)$	$F'_b \sin(k_y)$	$-F'_c \sin(k_z)$	0

Accounting for next-nearest-neighbor contributions, a (small) gap also opens in the case of hybridization with $m_J = 3/2$ and $5/2$ doublets, as can be seen from Table III, where we summarize coefficient functions now including next-nearest-neighbor contributions. Here we defined $F_a = F_{(y-z)}$, $F'_a = F_{-(y-z)}$, $F_b = F_{(x-z)}$, and $F'_b = F_{-(x-z)}$, with $F_{\pm(i\pm j)} = v_\parallel + v_{2\parallel}[1 \pm 2C_{i\pm j} - \sqrt{2}\cos(k_z)]$, $C_{i\pm j} = \sqrt{2}[\cos(k_i) \pm \cos(k_j)]$ $(i, j = x, y, z)$, and $F_c = 2v_\perp + v_{2\perp}(2 - C_{x+y})$, $F'_c = v_{2\perp}C_{x-y}$. Here $v_{\parallel/\perp}$ and $v_{2\parallel/2\perp}$ are the hybridization intensities within/perpendicular to the symmetry plane for first- and second-nearest-neighbor sites, respectively [as also used in Eq. (4) of the main text]. Notice that in this order of hopping approximation, effective models for $m_J = 3/2$ and $5/2$ doublets also show a chiral symmetry, i.e., γ_1 and γ_5, respectively. Including, however, contributions from third-nearest neighbors all coefficient functions become nonvanishing in the case of $m_J = 3/2$ and $5/2$ doublets. Only in the case of the $m_J = 1/2$ doublet h_5 remains zero. Finally, a discussion similar to the above applies to coefficient functions parametrizing hybridization with doublets from the $J = 7/2$ octet.

APPENDIX C: TETRAGONAL KONDO INSULATOR

We here focus on a tetragonal Kondo insulator with the $\Gamma^{5/2}_{1/2}$ doublet in the ground state and calculate the winding number from the nearest-neighbor model. Dispersion relations for conduction and (nearly) localized electrons then read $\varepsilon^{c,f}_{\boldsymbol{k}} = \varepsilon_{c,f} + 2t^{c,f}_\parallel[\cos(k_x) + \cos(k_y)] + 2t^{c,f}_\perp\cos(k_z)$, where $\varepsilon_{c,f}$ are the corresponding bands' center and $t^{c,f}_{\parallel/\perp}$ hopping parameters within/perpendicular to the symmetry plane of the tetragonal structure. Dispersion relations define coefficients $h_{0,4}(\boldsymbol{k})$ [see Eq. (2) in the main text] and coefficients $h^n_{1,2,3,5}(\boldsymbol{k})$ are taken, e.g., from Table II or III. With these functions Eq. (7) in the main text reads

$$N = \sum_{\boldsymbol{k}\in\boldsymbol{h}^{-1}(\boldsymbol{n}_0)} \mathrm{sgn}(-F_a F_b F_c \cos k_x \cos k_y \cos k_z), \tag{C1}$$

where $F_{a,b,c}$ have been discussed in the previous Appendix. To evaluate the sum (C1), it is then convenient to choose $\boldsymbol{n}_0 = h_4(0)\boldsymbol{e}_4$ whose preimage, $\boldsymbol{h}^{-1}(\boldsymbol{n}_0)$, is the eight

time-reversal-invariant points in the Brillouin zone. The result of this calculation is given in Eq. (8) of the main text.

APPENDIX D: SURFACE-STATE SPIN TEXTURE IN THE TETRAGONAL KONDO INSULATOR

The translationally invariant tetragonal Kondo insulators allows for a characterization in terms of winding number, as described in Eq. (7) in the main text and Appendix A. Here we apply the projection method to derive the surface Hamiltonian. Let us consider those time-reversal-invariant momenta points $\boldsymbol{k}_0$, as described in the previous Appendix. In their vicinity the Hamiltonian reads $\mathcal{H}(\boldsymbol{k}) = \sum_{i=1}^{3} v_i k_i \sigma_i \tau_x + m\tau_z$, with parameters v_i and m functions of $\boldsymbol{k}_0$. As an illustration we consider the surface Hamiltonian at $z = \pm L/2$, where L is the z-direction system size. Since translational invariance is broken in the z direction we substitute $k_z \to -i\partial_z$ and the zero-energy eigenfunctions are obtaining by

$$\left(\tau_z[m - (P_+ - P_-)v_z\partial_z] + \sum_{i=1}^{2} v_i k_i \sigma_i \tau_x\right)\psi_{\boldsymbol{k}}(z) = 0, \quad \text{(D1)}$$

where we have introduced the projection operators $P_\pm = \frac{1}{2}(\mathbb{I} \pm \sigma_z\tau_y)$. The spatially dependent part of the Schrödinger equation, with $\psi_{\boldsymbol{k}}(z) = \psi(z)\psi(\boldsymbol{k})$, is solved by eigenfunctions of $P_\pm$; that is, introducing $P_\pm\psi^\pm = \pm\psi^\pm$ the z-coordinate-dependent part reads

$$\psi(z) = e^{\frac{m}{v_z}z}\psi^+ + e^{-\frac{m}{v_z}z}\psi^-. \quad \text{(D2)}$$

Depending on the sign of $\mathrm{sgn}(m/v_z) = \pm$ the first/second contribution accounts for the wave functions exponentially localized at $z = \mp L/2$. Concentrating on either one of the surfaces we project the $\boldsymbol{k}$-dependent part on the corresponding eigenspace $H^\pm \equiv P_\pm H(\boldsymbol{k}) P_\pm$. In order to find an explicit expression it is convenient to introduce $U \equiv e^{i\frac{\pi}{4}\tau_x}$ such that the surface Hamiltonians are written in the rotated basis $H_U^\pm = U^\dagger H^\pm U$, explicitly

$$H_U^+ = \begin{pmatrix} 0 & 0 & 0 & v_x k_x - i v_y k_y \\ 0 & 0 & 0 & 0 \\ 0 & 0 & 0 & 0 \\ v_x k_x + i v_y k_y & 0 & 0 & 0 \end{pmatrix}, \quad \text{(D3)}$$

$$H_U^- = \begin{pmatrix} 0 & 0 & 0 & 0 \\ 0 & 0 & v_x k_x + i v_y k_y & 0 \\ 0 & v_x k_x - i v_y k_y & 0 & 0 \\ 0 & 0 & 0 & 0 \end{pmatrix}. \quad \text{(D4)}$$

From this result we notice that each of the two Hamiltonians describes a given surface depending on $\mathrm{sgn}[m(\boldsymbol{k}_0)v_z(\boldsymbol{k}_0)]$. The surface Hamiltonians on opposite surfaces have opposite chiralities, i.e., $\mathrm{ch}_+ = \mathrm{sgn}(v_x v_y)$ and $\mathrm{ch}_+ = -\mathrm{sgn}(v_x v_y)$. Thus, the chirality of the surface states at a given surface is fixed by the product $\mathrm{ch} = \mathrm{sgn}(m v_x v_y v_z)$. Coming back to our example in the previous section, the sum is over time-reversal-invariant momenta where band inversion occurs, i.e., $m(\boldsymbol{k}_0) < 0$. Having fixed the Brouwer's formula $\boldsymbol{n}_0 = h_4(0)\boldsymbol{e}_4$ we notice that each summand is related to the chirality of surface states such that

$$N = \sum_{\boldsymbol{k}_0} \mathrm{sgn}[-v_x(\boldsymbol{k}_0)v_y(\boldsymbol{k}_0)v_z(\boldsymbol{k}_0)]. \quad \text{(D5)}$$

The absolute value of the winding accounts for the total chirality of surface states when present on a given surface. The latter is a well-defined quantity, i.e., independent of the surface one looks at.

APPENDIX E: CUBIC KONDO INSULATOR AT LOW NEIGHBOR HOPPING APPROXIMATION

As an example of the low neighbor hopping approximation, we apply our calculations to the 4-band model of a cubic structure as described in Ref. [12]. According to our notation, their Hamiltonian can be rewritten as $\varepsilon_{\boldsymbol{k}}^{c,f} = \epsilon_0^{c,f} - 2t_{c,f}\eta_1^{c,f}(c_x + c_y + c_z) - 4t_{c,f}\eta_2^{c,f}(c_x c_y + c_y c_z + c_z c_x)$, where $\varepsilon_{\boldsymbol{k}}^{c,f}$ are dispersion relations for the conducting and localized bands, $\epsilon_0^{c,f}$ are the corresponding bands' center, and $t_{c,f}\eta_1^{c,f}$ and $t_{c,f}\eta_2^{c,f}$ are the bandwidths for the first- and second-nearest neighbors, respectively; finally, $c_i = \cos(k_i)$ with $i = x, y, z$. Using the notation of Table III with $n = 1$, the hybridization elements have their coefficient functions as $F_a = -2V[\eta^{v1} + \eta^{v2}(c_y + c_z)]$, $F_b = -2V[\eta^{v1} + \eta^{v2}(c_x + c_z)]$, and $F_c = 2V[\eta^{v1} + \eta^{v2}(c_y + c_x)]$, where $V\eta^{v1}$ and $V\eta^{v2}$ are the hybridization amplitudes for nearest- and next-nearest-neighbor hopping, respectively. Finally, the parameters were set to $\epsilon_0^f - \epsilon_0^c = -2eV$, $t_c = 1eV$, $t_f = 0.003eV$, $\eta_1^c = \eta_1^f = 1$, $\eta_2^c = \eta_2^f = -0.5$, $V\eta^{v1} = 0.2eV$, and $V\eta^{v2} = 0$.

Now we intend to calculate the winding number according to Eq. (C1), where we evaluate the sum by choosing $\boldsymbol{n}_0 = -h_4(0)\boldsymbol{e}_4$, whose preimage is the eight time-reversal-invariant points in the Brillouin zone. The result of this calculation is $N = +3$, which characterizes the three Dirac cones with the same pseudospin chirality in Fig. 3(a) in Ref. [12].

[1] M. Dzero, K. Sun, V. Galitski, and P. Coleman, Phys. Rev. Lett. **104**, 106408 (2010).

[2] T. Takimoto, J. Phys. Soc. Jpn. **80**, 123710 (2011).

[3] M. Dzero, K. Sun, P. Coleman, and V. Galitski, Phys. Rev. B **85**, 045130 (2012).

[4] M. Fruchart and D. Carpentier, C. R. Phys. **14**, 779 (2013).

[5] M. Dzero and V. Galitski, J. Exp. Theor. Phys. **117**, 499 (2013).

[6] D. J. Kim, J. Xia, and Z. Fisk, Nat. Mater. **13**, 466 (2014).

[7] G. Li, Z. Xiang, F. Yu, T. Asaba, B. Lawson, P. Cai, C. Tinsman, A. Berkley, S. Wolgast, Y. S. Eo, D.-J. Kim, C. Kurdak, J. W. Allen, K. Sun, X. H. Chen, Y. Y. Wang, Z. Fisk, and L. Li, Science **346**, 1208 (2014).

[8] M. Dzero, J. Xia, V. Galitski, and P. Coleman, Annu. Rev. Condens. Matter Phys. **7**, 249 (2016).

[9] V. Alexandrov, M. Dzero, and P. Coleman, Phys. Rev. Lett. **111**, 226403 (2013).

[10] M. Legner, A. Rüegg, and M. Sigrist, Phys. Rev. B **89**, 085110 (2014).

[11] P. P. Baruselli and M. Vojta, Phys. Rev. B **90**, 201106 (2014).

[12] P. P. Baruselli and M. Vojta, Phys. Rev. Lett. **115**, 156404 (2015).

[13] M. Legner, A. Rüegg, and M. Sigrist, Phys. Rev. Lett. **115**, 156405 (2015).

[14] N. Xu, P. K. Biswas, J. H. Dil, R. S. Dhaka, G. Landolt, S. Muff, C. E. Matt, X. Shi, N. C. Plumb, M. Radović, E. Pomjakushina, K. Conder, A. Amato, S. V. Borisenko, R. Yu, H. M. Weng, Z. Fang, X. Dai, J. Mesot, H. Ding, and M. Shi, Nat. Commun. **5**, 4566 (2014).

[15] Y. Zhong, Y.-F. Wang, H.-T. Lu, and H.-G. Luo, Phys. Rev. B **88**, 235111 (2013).

[16] T. Yoshida, R. Peters, S. Fujimoto, and N. Kawakami, Phys. Rev. B **87**, 165109 (2013).

[17] J. Werner and F. F. Assaad, Phys. Rev. B **88**, 035113 (2013).

[18] G. Baskaran, arXiv:1507.03477.

[19] A. Thomson and S. Sachdev, Phys. Rev. B **93**, 125103 (2016).

[20] A. M. Lobos, A. O. Dobry, and V. Galitski, Phys. Rev. X **5**, 021017 (2015).

[21] Y. Zhong, Y. Liu, and H.-G. Luo, Eur. Phys. J. B **90**, 147 (2017).

[22] Inversion symmetry $\mathcal{I}\mathcal{H}_{\mathbf{k}}\mathcal{I}^{-1} = \mathcal{H}_{-\mathbf{k}}$ restricts the diagonal blocks of $\mathcal{H}_{\mathbf{k}}$ in orbital space to be even, and off-diagonal hybridization blocks to be odd functions in $\mathbf{k}$. In the presence of time-reversal symmetry, $\mathcal{T}\mathcal{H}_{\mathbf{k}}\mathcal{T}^{-1} = \mathcal{H}_{-\mathbf{k}}$, this excludes Pauli-spin matrices on the orbital diagonal blocks of $\mathcal{H}$, while restrictions on hybridization blocks are different for symmetric and antisymmetric hybridization combinations $c^{\dagger}f \pm f^{\dagger}c$; i.e., symmetric elements involve Pauli spin matrices while antisymmetric elements are independent of spin orientations. Notice that the choice of a relative phase factor between c and f electrons, for which $\mathcal{T}$ is of the indicated form, is reflected in coefficients $c_m, \bar{c}_m$ in Eq. (3), and one may alternatively work in a basis where $\mathcal{T} = \tau_3 \otimes i\sigma_2 K$.

[23] T. Yamada and Y. Ono, Phys. Rev. B **85**, 165114 (2012).

[24] That is, without negative signs in the first line, and c_n, $\bar{c}_n$ now purely real/imaginary numbers for n odd/even.

[25] For $J = 7/2$ it is the matrices γ_i with $i = 1, 2, 5$.

[26] A. P. Schnyder, S. Ryu, A. Furusaki, and A. W. W. Ludwig, Phys. Rev. B **78**, 195125 (2008).

[27] M. Sato and Y. Ando, Rep. Prog. Phys. **80**, 076501 (2017).

[28] See the Appendices, where we review the Brouwer index, give details on hybridization matrices, discuss the tetragonal Kondo insulator, and exemplify a nonzero winding number with spin textures in cubic structures.

[29] Such perturbations change class DIII to AIII without modifying its characterizing topological invariant.

[30] L. Fu and C. L. Kane, Phys. Rev. B **76**, 045302 (2007).

[31] The renormalization factor is, e.g., found from expanding the self-energy due to interaction between localized f electrons close to the Fermi surface [3], or alternatively using slave bosons [32] or Gutzwiller's approximation [33,34].

[32] H. Kusunose, S. Yotsuhashi, and K. Miyake, Phys. Rev. B **62**, 4403 (2000).

[33] T. M. Rice and K. Ueda, Phys. Rev. Lett. **55**, 995 (1985).

[34] T. M. Rice and K. Ueda, Phys. Rev. Lett. **55**, 2093 (1985).

[35] G. Rosenberg and M. Franz, Phys. Rev. B **82**, 035105 (2010).

[36] J. I. Väyrynen and G. E. Volovik, JETP Lett. **93**, 344 (2011).

[37] S. Shen, in *Topological Insulators: Dirac Equation in Condensed Matters*, Springer Series in Solid-State Sciences, Vol. 174 (Springer, Singapore, 2013).

[38] E. Fradkin, *Field Theories of Condensed Matter Physics*, 2nd ed. (Cambridge University Press, New York, 2013).

[39] C. J. Bradley and A. P. Cracknell, *The Mathematical Theory of Symmetry in Solids: Representation Theory for Point Groups and Space Groups* (Oxford Clarendon Press, New York, 1972).

[40] S. Paschen, H. Winkler, T. Nezu, M. Kriegisch, G. Hilscher, J. Custers, A. Prokofiev, and A. Strydom, J. Phys.: Conf. Ser. **200**, 012156 (2010).

[41] M. Sundermann, F. Strigari, T. Willers, H. Winkler, A. Prokofiev, J. M. Ablett, J.-P. Rueff, D. Schmitz, E. Weschke, M. M. Sala, A. Al-Zein, A. Tanaka, M. W. Haverkort, D. Kasinathan, L. H. Tjeng, S. Paschen, and A. Severing, Sci. Rep. **5**, 17937 (2015).

[42] M. Sundermann, K. Chen, Y. Utsumi, Y.-H. Wu, K.-D. Tsuei, J. Haenel, A. Prokofiev, S. Paschen, A. Tanaka, L. H. Tjeng, and A. Severing, J. Phys.: Conf. Ser. **807**, 022001 (2017).

[43] For a DMFT study on this compound, discussing the temperature dependence on the selecting ground state, see, e.g., Ref. [46].

[44] T. Yamashita, R. Miyazaki, Y. Aoki, and S. Ohara, J. Phys. Soc. Jpn. **81**, 034705 (2012).

[45] B. J. Kim, H. Jin, S. J. Moon, J.-Y. Kim, B.-G. Park, C. S. Leem, J. Yu, T. W. Noh, C. Kim, S.-J. Oh, J.-H. Park, V. Durairaj, G. Cao, and E. Rotenberg, Phys. Rev. Lett. **101**, 076402 (2008).

[46] P. Wissgott and K. Held, Eur. Phys. J. B **89**, 5 (2016).

[47] M.-T. Tran, T. Takimoto, and K.-S. Kim, Phys. Rev. B **85**, 125128 (2012).